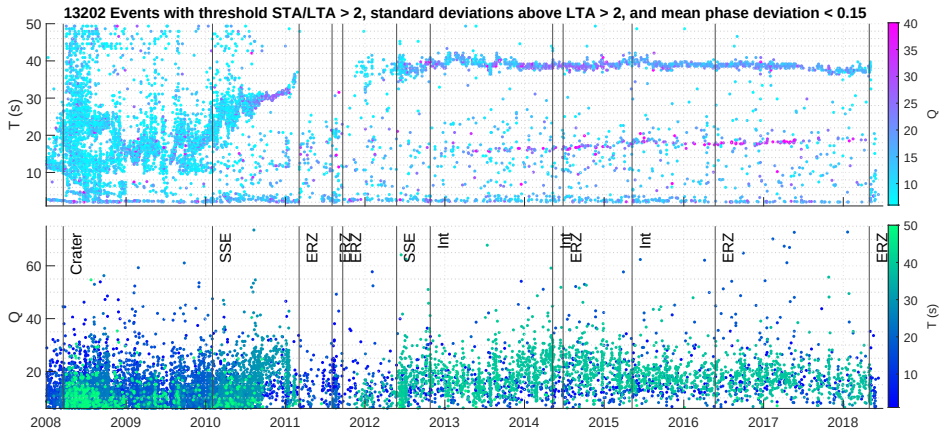

Figure S7. Resonant signal catalog from 2008-2018 with less strict event detection thresholds than presented in the main text yielding ∼13,000 events. The thresholds used in this version are: STA/LTA > 2, standard deviations above the LTA > 2, $Q > 4$, and mean phase deviation < 0.15 radians. 'Crater' indicates where the Halema'uma'u crater first formed, 'SSE' indicates slow slip events, 'Int' indicates documented summit intrusions, and 'ERZ' indicates eruptions along the East-Rift-Zone.

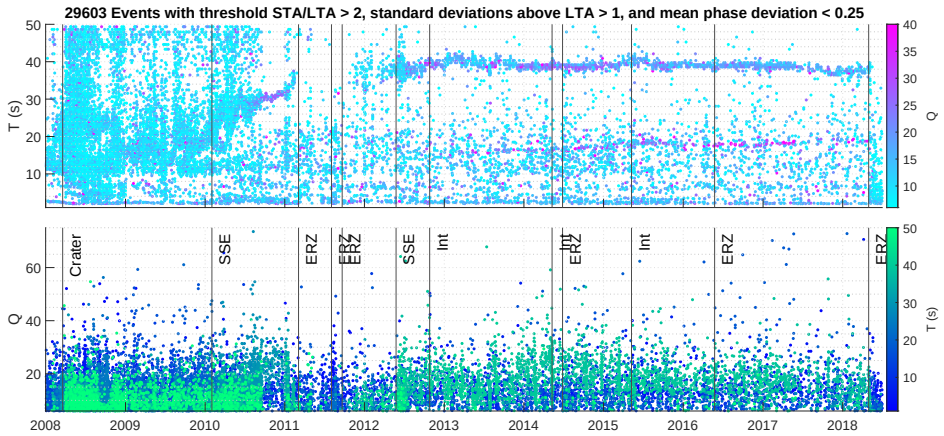

Figure S8. Resonant signal catalog from 2008-2018 with less strict event detection thresholds than presented in the main text yielding ∼30,000 events. The thresholds used in this version are: STA/LTA > 2, standard deviations above the LTA > 1, $Q > 4$, and mean phase deviation < 0.25 radians. 'Crater' indicates where the Halema'uma'u crater first formed, 'SSE' indicates slow slip events, 'Int' indicates documented summit intrusions, and 'ERZ' indicates eruptions along the East-Rift-Zone.

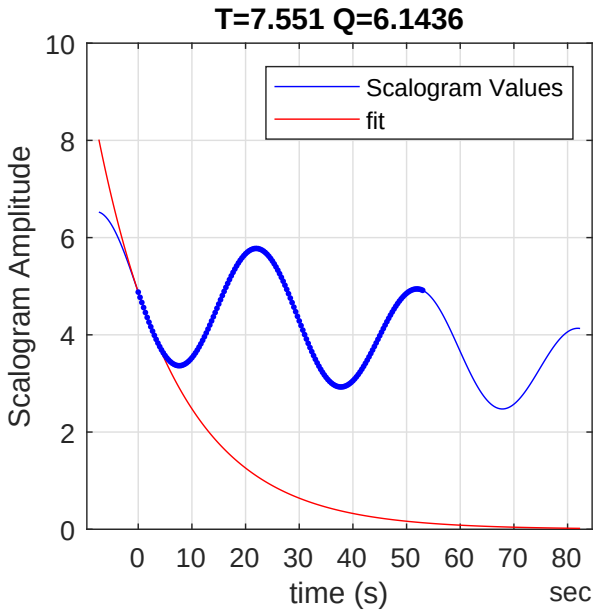

Figure S9. Example estimation of Q by scalogram exponential fit. Applied to synthetic seismograms consisting of a series of tapered step displacements (velocity spikes) spaced 30 s apart, plus white noise from a standard normal distribution scaled by 0.1% of the signal amplitude. The closely spaced spikes create a Dirac comb effect, where the frequency spectrum would indicate apparent resonances at 15 s, 7.5 s, 3.25 s, and etc. The time resolution of the β=20 wavelet we use for calculating Q is sufficient to distinguish gaps in this apparent 7.5 s resonance, so our fit avoids overestimating Q as a standard least-squares exponential regression would.

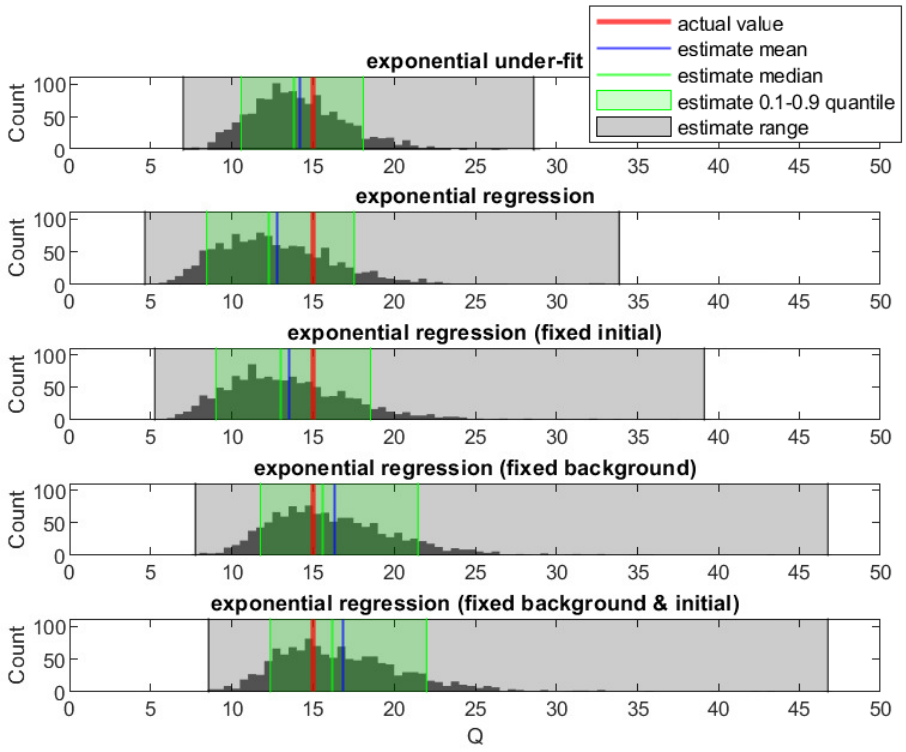

Figure S10. Comparison of exponential fit methods for estimating Q from 1255 synthetic seismograms with different random noise. These seismograms consist of a VLP signal with $[T, Q] = [20\text{ s}, 15]$, plus white noise from a standard normal distribution scaled by 200% of the signal amplitude. All of the methods work well at low noise levels; at the high noise levels used here the Sompi AR method generally does not detect resonance and so is not shown for comparison. 'Under-fit' is the fit we use (Eq. 2, Fig. 6), the other fits are least-squares exponential regressions with various parameters fixed. 'Initial' means amplitude at the first time being fit (t_1) is fixed to the CWT amplitude at that time. 'Background' means the asymptotic value approached as time goes to infinity is fixed to the minimum noise value in the full 4 hr time window. While the 'under-fit' has a bias towards smaller Q, this bias is small (less than 2 in these simulations) and the spread is smaller than any of the other fitting approaches.

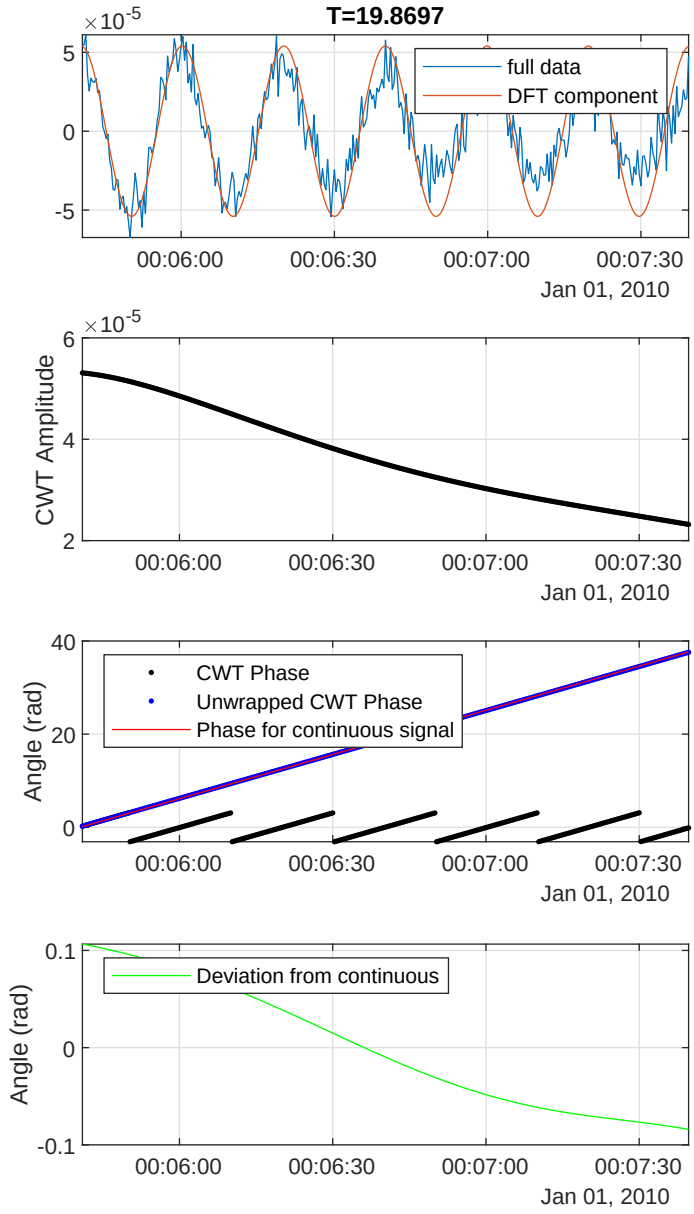

Figure S11. Example phase continuity from a synthetic seismogram consisting of a resonant signal with T=20 s and Q=20, plus white noise from a standard normal distribution scaled by 0.1% of the signal amplitude. In this case the phase deviation is small (mean of around 0.05 radians), correctly indicating that this is likely a continuous oscillation.

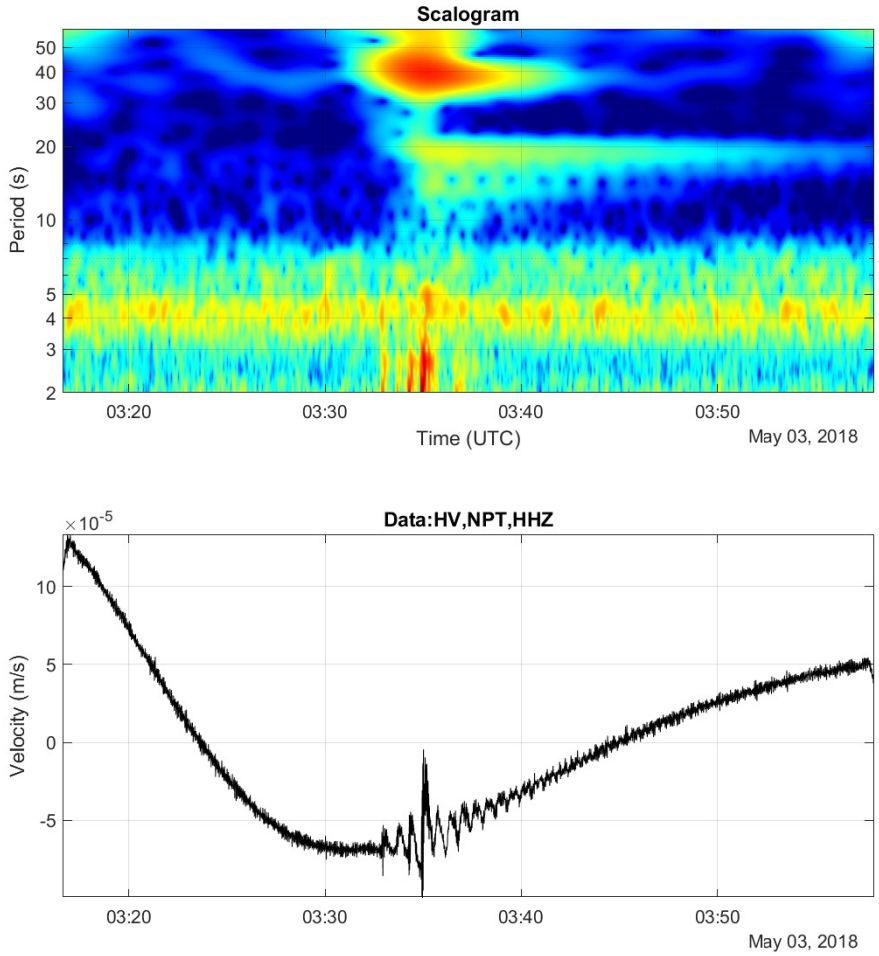

Figure S12. VLP event with two clear lava-lake-sloshing modes from May 2018, a day after the lava-lake began draining. The dominant 40 s mode for this event started with impulsive inflationary motions, though with only a very faint high frequency trigger, but then grew for several minutes until a second impulse occurred and exponential decay began. The lava-lake-sloshing modes appeared alongside this second impulse.

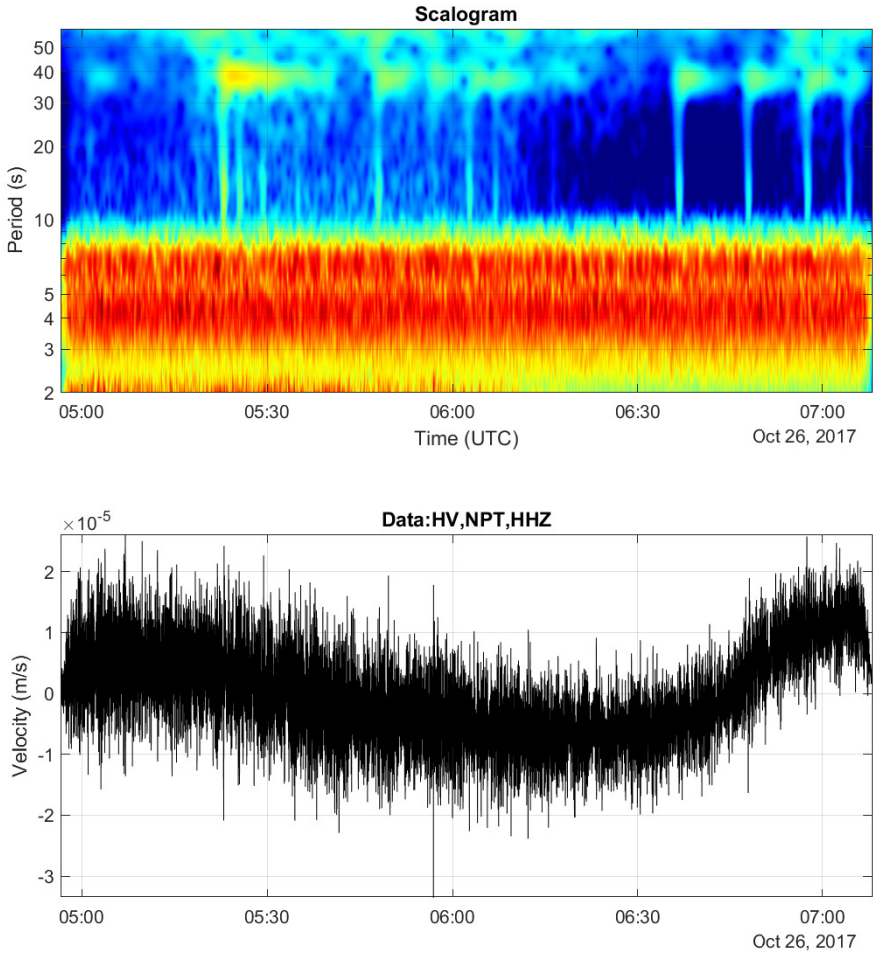

Figure S13. Closely spaced Normal conduit-reservoir events from October 2017.

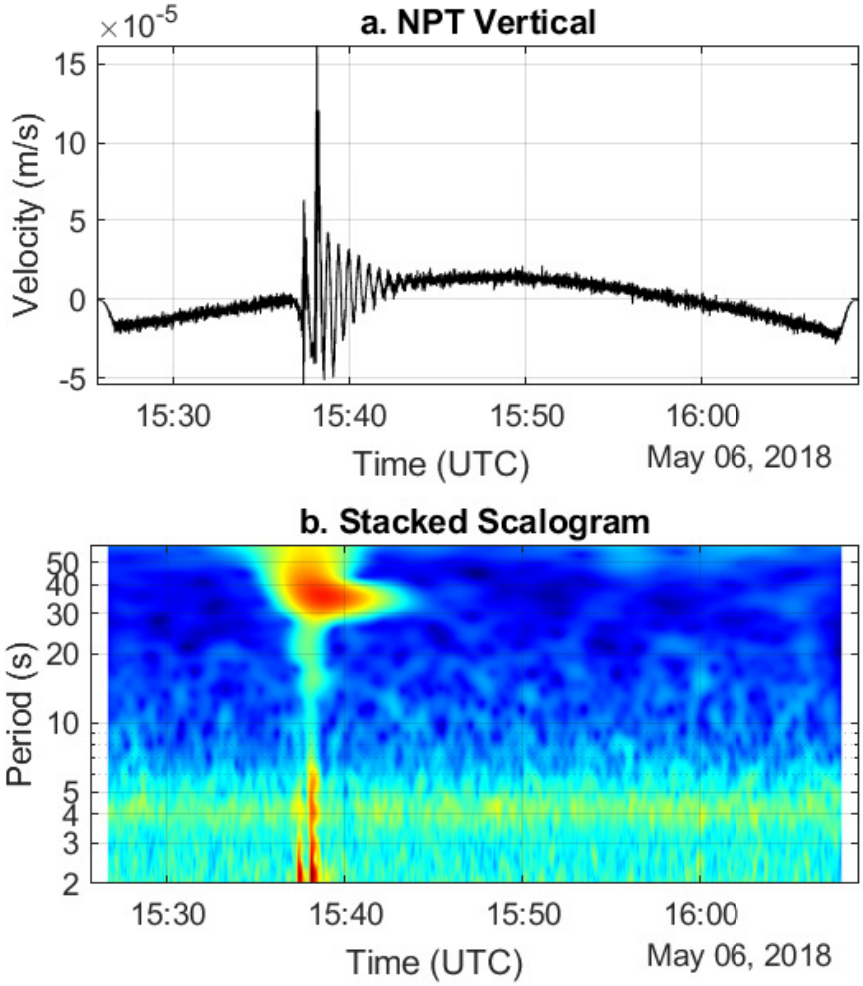

Figure S14. Normal VLP event from May 2018, 4 days after the lava-lake began draining. This event exhibited a distinctly lower T than preceding events (35 s as compared to 37-40 s), and is the last event conduit-reservoir event recorded in our catalog. This event started with an impulsive inflation, though with minimal broadband energy. Another larger broadband impulse occurred a minute later that corresponded to increased oscillation amplitude, after which the oscillation decayed exponentially.

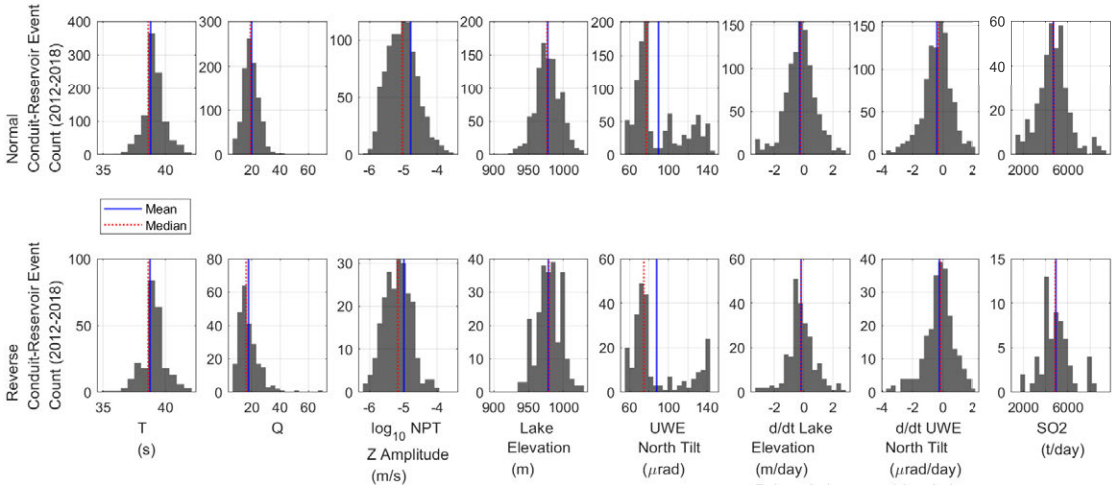

Figure S15. Histograms of Normal and Reverse conduit-reservoir mode event parameters from 2012-2018.